

Multi-Objective Optimization of Blades for Fixed Pitch Horizontal Axis Tidal Stream Turbines with Variable Speed Control

Nicholas Kaufmann^{#1}, Thomas H. Carolus^{#2}, Ralf Starzmann^{*3}

[#]*Institute for Fluid- and Thermodynamics, University of Siegen.*

57068 Siegen, Germany

¹nicholas.kaufmann@uni-siegen.de

²thomas.carouls@uni-siegen.de

^{*}*SCHOTTEL HYDRO GmbH, Mainzer Straße 99,*

56322 Spay, Germany

³rstarzmann@schottel.de

Abstract— The objectives of this contribution is an enhanced design method of 3D blade geometries for fixed pitch horizontal axis tidal turbines with variable speed control, simultaneously targeting at maximum power output, minimum thrust load and an extended cavitation free range of operation. To optimize the blade's spanwise twist and chord distribution, an extended BEM code, allowing the prediction of the performance characteristics including cavitation inception, was coupled to an evolutionary algorithm, capable of global multi-objective optimization.

A case study is performed resulting in a set of novel blade geometries, providing optimum trade-offs between power, thrust and cavitation sensitivity. The comparison to an analytically designed rotor using standard design method showed that the presented optimization method yields rotor geometries with significantly lower thrust loads and cavitation sensitivity as compared to the analytical blade design.

While the BEM performance prediction model was validated successfully through experiments, a validation of the novel, optimization based design method has to be carried out in a future step.

Keywords— Tidal stream turbine, rotor blade design, multi-objective optimization, blade element momentum theory

I. INTRODUCTION

There is an increasing interest in small horizontal axis free stream turbines, for instance to harvest energy from tidal currents. They are thought to be an alternative to large scale and hence capital-intensive turbines. Typical rotor diameters are 3 to 6 m. In order to keep the cost low and the design robust, no blade pitch mechanism is included, i.e. they are fixed-pitch designs. The preferred control of fixed-pitch turbines is some type of variable speed, known for many years in the turbine community. For instance, an advanced variable speed control is realized in the commercially available SCHOTTEL HYDRO SIT250 [1]. For an introductory illustration it is sufficient to consider the fundamental concept of variable speed control and to rely on synthetic turbine

characteristics, i.e. simplified non-dimensional power and thrust characteristics of a turbine as in Fig. 1 in terms of - tip speed ratio

$$\lambda \equiv \frac{u_{tip}}{c_0} \quad (1)$$

- power coefficient

$$C_P \equiv \frac{P}{0.5\rho c_0^3 A}, \quad (2)$$

- thrust coefficient

$$C_T \equiv \frac{F_{ax}}{0.5\rho c_0^2 A} \quad (3)$$

- cavitation number

$$\sigma_{0.7} \equiv \frac{P_{atm} + \rho g h_{hub} - p_v}{0.5\rho c_0^2 (1 + (0.7\lambda)^2)}. \quad (4)$$

P is the shaft power available from the turbine, F_{ax} the thrust on the rotor. The tip speed is obtained from the rotor diameter and its rotational speed $u_{tip} = r_{tip}\Omega = \pi d_{tip}n$, $A = \pi(d_{tip}/2)^2$ is the swept area of the rotor and c_0 the free flow velocity far upstream of the turbine. p_v is the vapor pressure of the fluid, p_{atm} the atmospheric pressure, g the gravity and h_{hub} the immersion depth of the hub. Cavitation is avoided when the cavitation number exceeds a critical value $\sigma_{0.7,crit}$. For any chosen rotor speed the two non-dimensional characteristics $C_P(\lambda)$ and $C_T(\lambda)$ can be converted into dimensional power and thrust curves as a function of c_0 , plotted as blue dotted lines in Fig. 2. The red solid lines in Fig. 2 connect all optimum operating points for each rotor speed, i.e. where $\lambda = \lambda_{opt} = \text{const}$. Preferably, the turbine is operated along these red lines. However, as c_0 exceeds $c_{0,rated}$ the controller increases the rotor speed to limit the turbine power to a preset threshold P_{rated} . This so called overspeed control unavoidably leads to an operating tip speed ratio of the turbine $\lambda_{overspeed} > \lambda_{opt}$ and

hence to an undesired increase of thrust T (lower diagram in Fig. 2).

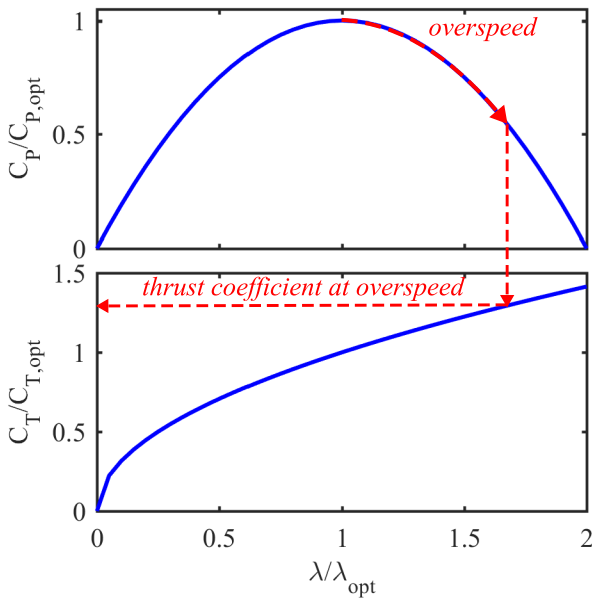


Fig.1 Synthetic simplified non-dimensional power and thrust characteristics of a turbine (schematically)

overspeed operating points. Hence a target is to identify turbine designs with a very flat or even negative slope of the $C_T(\lambda)$ characteristic for $\lambda > \lambda_{opt}$ while keeping $C_{P,opt}$ as close as possible to its theoretical maximum. A similar analysis for the cavitation inception characteristic yields a third target: σ_{crit} should be as low as possible at λ_{opt} and $\lambda > \lambda_{opt}$ to minimize the required immersion depth of the turbine or enlarge the allowable inflow velocity range for a given immersion depth.

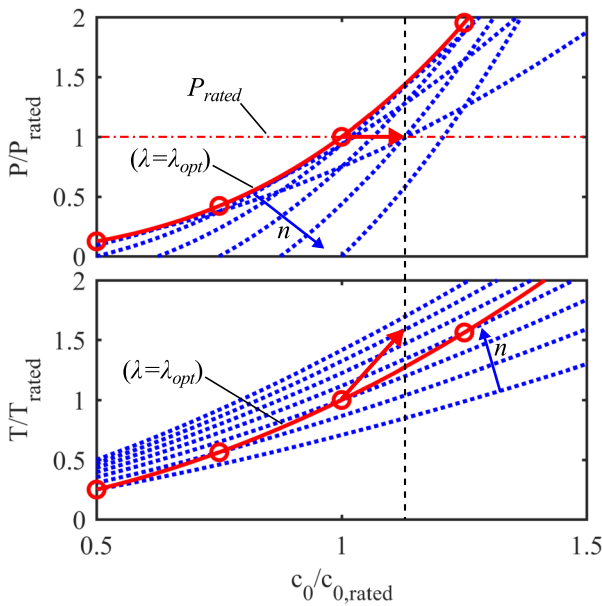
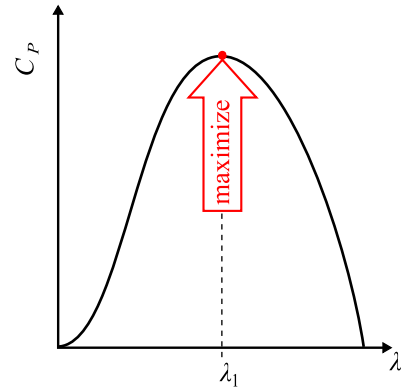
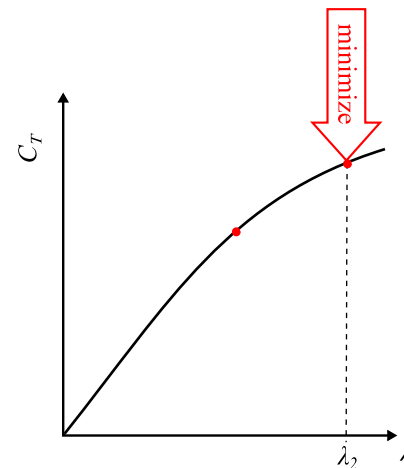


Fig. 2 Dimensional power and thrust characteristics for different rotor speeds (derived from the synthetic simplified non-dimensional characteristics in Fig. 2). A controller drives the turbine into overspeed to limit the power output to P_{rated} . The red circles indicate optimum operating points for each rotor speed, i.e. where $\lambda = \lambda_{opt}$.



It is important to note that the rate of increase of thrust depends not only on rotor speed but also on the slope of the non-dimensional $C_T(\lambda)$ characteristic in overspeed conditions; obviously, the less steep the slope, the lower is the thrust in

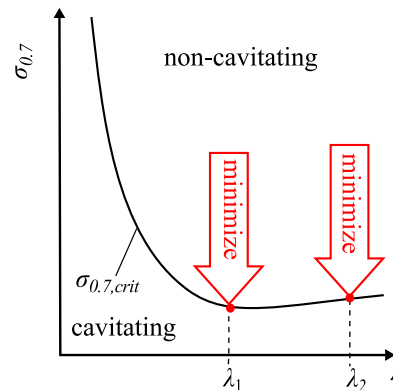


Fig. 3 Non-dimensional turbine performance characteristics and design targets

This leads to design targets as summarized in Fig. 3 in terms of non-dimensional turbine characteristics. Not only one single value such as $C_{P,opt}$, but the shapes and levels of all three turbine performance characteristics are relevant. Most likely there is a trade-off between power output, thrust, non-cavitating operating range.

The overall objectives of this work is a multi-objective optimization scheme yielding an optimal 3D blade geometry for fixed pitch horizontal axis tidal turbines with variable speed control.

II. LITERATURE SURVEY

Design methods of axial tidal turbine blades are very similar to those of wind turbines. Pioneers of the widely used blade element momentum theory (BEM) are GLAUERT [2] and SCHMITZ [3]. BEM can also be used as an integral part of a *performance prediction* scheme for any existing turbine. An application to tidal turbines has been published e.g. by BATTEN et al [4] and MASTERS et al [5].

Da SILVA et al [6], GOUNDAR and AHMED [7], WU et al. [8] expanded the GLAUERT/SCHMITZ design method by integrating a cavitation model. Modifications of blade geometry obtained from these models, for instance larger chord lengths at the blade outer region, led to improved cavitation property of a particular turbine in one targeted design point.

However, as already explained above, fixed-pitch turbines with their speed control are operated along a large range of operating points. Hence, the limitations of the existing design methods are obvious, as pointed out by ARNOLD et al [9] and SALE et al [10]. SALE et al, for instance, designed a stall-regulated tidal turbine via a combination of a fundamental BEM method with a genetic algorithm. Their optimization aimed for a maximum power output at rotor design speed and all relevant off-design speeds during control. Cavitation inception was assessed during the optimization - candidate designs with inadmissible cavitation properties were dismissed. RUOPP et al. [11] targeted at maximum power while limiting the thrust to a pre-defined value. The turbine performance was calculated utilizing a 3D RANS simulation which was coupled to a genetic optimization algorithm. A multi-objective optimization with respect to power and thrust coefficient has been carried out by HUANG and KANEMOTO in [12]. They applied a response surface method (RSM) to the NSGA-II algorithm by DEB et al. [13]. Cavitation has not been considered.

Although these design methods enable to address one or two of the design targets (i) power output, (ii) thrust and (iii) cavitation separately, they had been applied successfully, for instance for the design of the SCHOTTEL HYDRO SIT250 tidal stream turbine, presented in section III and depicted in

Fig. 6. Nevertheless, further progress is expected from a true multi-objective optimization of the three conflicting targets.

III. METHODOLOGY

Fig. 4 shows a schematic flow diagram of the complete design scheme presented in this contribution. The key ingredients are

- a semi-empirical performance prediction model (*BEM model*)
- an optimization method (*evolutionary algorithm*)

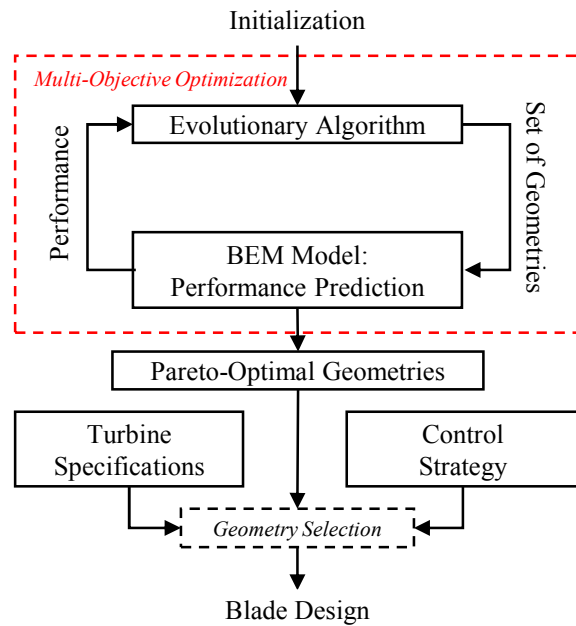


Fig. 4 Complete design scheme based on a semi-analytical performance prediction model, embedded in a multi-objective algorithm

To initialize an optimization, rotor tip and hub diameter, inflow velocity and specifications of the fixed blade parameters have to be defined. The evolutionary algorithm (EA) yields a set of blade geometries for which the performance at the specified operating points is evaluated by the BEM model. Based on the performance, the EA updates the subsequent geometry set aiming for a further improved performance. The result of the multi-objective optimization is a set of geometries representing the optimal trade-offs between the conflicting design targets (*Pareto-set*). Finally, taking into account constraints and the control strategy chosen, the optimal design from the *Pareto-set* can be selected. The systematic selection of one optimal rotor geometry for a specific application will not be part of this paper, since we focus on the multi-objective optimization only.

A. A Validated Semi-empirical Performance Prediction Model

Here we use an enhanced in-house blade element momentum (BEM) method - briefly summarized in the next paragraph - for the prediction of the performance and critical cavitation number of a given turbine.

In spanwise direction the turbine blade is segmented into a number of blade elements (BE). For every BE, the local power and thrust coefficients are derived based on momentum conservation ($C_{P,M}$ and $C_{T,M}$) and the dynamic forces on a hydrofoil ($C_{P,DF}$ and $C_{T,DF}$). Equating $C_{P,M} = C_{P,DF}$ and $C_{T,M} = C_{T,DF}$ yields two nonlinear equations for the unknown local axial and tangential velocity components and eventually the BEs' C_P and C_T . The overall turbine performance at a specific tip speed ratio then results from a summation over all BEs.

Simplifying assumptions, such as a flow field that is purely 2-D, are limiting the precision of the basic BEM theory. In order to increase the accuracy of the method, various submodels are applied. BUHL's [14] correction of the thrust coefficient for large axial flow retardation is used, furthermore models by PRANDTL/GLAUERT [2] and SHEN [15] accounting for blade hub and tip losses.

The hydrodynamic forces (lift and drag) for all BEs are needed to determine $C_{P,DF}$ and $C_{T,DF}$. Since lift and drag of the hydrofoil sections are functions of the Reynolds number Re and angle of attack α , they are calculated in advance and stored in a database. These polar data are obtained utilizing the public domain code XFOIL by DRELA [16]. To mimic an incompressible flow, the Mach number is set to zero. The transition from a laminar to turbulent boundary is calculated using the e^n -method with a threshold amplification ratio of $N_{crit} = 1$, which corresponds to a free stream turbulence level of 2% [17]. Post-stall data are extrapolated according to VITERNA et al. [18]. Although VITERNA's correlation is empirical and known for its limited accuracy, it ensures numerical stability.

Cavitation in a turbine is a very complex phenomenon and affected by a variety of factors, which naturally cannot all be accounted for within a semi-analytic BEM method. The cavitation number $\sigma_{0.7}$ introduced in eq. (3) is solely a function of the turbine's operating conditions, independent of the blade shape. As mentioned above, cavitation is avoided when the cavitation number exceeds a critical value $\sigma_{0.7,crit}$. Hence, for a given rotor geometry, the turbine's cavitation characteristic is given by $\sigma_{0.7,crit}(\lambda)$, schematically shown in Fig. 5. For each λ the value of $\sigma_{0.7}$, where cavitation inception is observed, is defined as $\sigma_{0.7,crit}$. It is usually determined experimentally in a cavitation tunnel by varying the static pressure. For designing or optimizing a rotor blade, the a priori prediction of $\sigma_{0.7,crit}(\lambda)$ is crucial. Cavitation may occur on the blade suction surface and near the blade tip region due to the presence of the tip vortex. Typically, the onset of tip vortex cavitation is prior to blade suction surface cavitation. Since tip vortex cavitation does rarely harm the blade structure nor degrade the turbine performance, we concentrate on the blade suction surface cavitation. Then, an estimate of the turbine cavitation characteristics can be made on the basis of the chordwise

pressure distributions of the BEs which are linked to lift and drag. These pressure distributions are also taken from XFOIL, accepting that 3-D effects are not resolved.

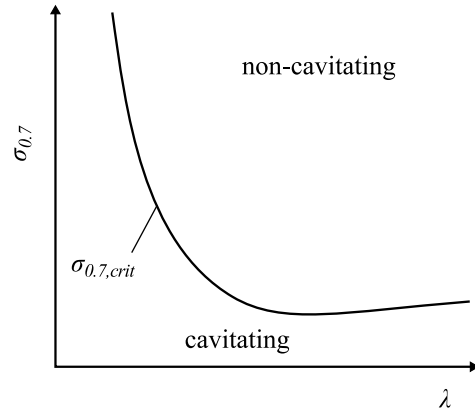


Fig.5 Critical cavitation number as a function of tip-speed ratio (schematically)

A validation of the performance prediction model is presented for the 1:8 model scale fixed pitch SCHOTTEL HYDRO Instream Turbine 250 (SIT250), Fig. 6. It is a three-bladed turbine with a design tip-speed ratio $\lambda = 5$. The rotor diameter of the 1:8 scale model is 0.5 m. It is CNC-milled from brass. Since this turbine was originally designed by the first author of this paper, the full geometry of all blade elements forming the blade is known in detail, but cannot be published due to commercial interests. All model scale experiments were performed at the Schiffbau-Versuchsanstalt Potsdam GmbH (SVA Potsdam).



Fig. 6: 1:8 scaled brass model of the SCHOTTEL SIT250 for the validation experiments

The most relevant data of the towing tank are compiled in Table I. The shaft of the turbine is immersed one rotor diameter below the waterline. The cross-sectional blockage of

the open water tests was 0.5%. For cavitation studies the turbine is placed in a cavitation tunnel with a specification as in Table II.

The basic testing procedure in the towing tank and the cavitation tunnel is the same. Tests were carried out over a range of tip speed ratios, which had been achieved by varying the rotational speed of the turbine for a given inflow velocity. 10 s- time records of thrust, torque, rotational speed and inflow speed were recorded synchronously, allowing an assessment of accuracy. According to the recommendations of the International Towing Tank Conference (ITTC) [28], the measured values for thrust and torque were corrected using a dummy hub of the same mass of the model turbine.

TABLE I
SVA TOWING TANK FACILITY

Towing tank dimensions	280.0 m length 9.0 m width 4.5 m depth
Maximum carriage velocity (corresponding to c_0)	7.0 m/s
Dynamometer type H39, Kempf and Remmers	$n_{max} = 60 \text{ s}^{-1}$ $T_{max} = 1000 \text{ N}$ $Q_{max} = 50 \text{ Nm}$
Shaft immersion depth	0.5 m

TABLE II
SVA CAVITATION TUNNEL TEST FACILITY

Cavitation tunnel test section (length)	2600 mm
Cavitation tunnel test section (cross section)	850 mm x 850 mm
Pressure variation	950 mbar – 1200 mbar
Maximum flow velocity (corresponding to c_0)	7.5 m/s
Dynamometer H36, Kempf and Remmers	$n_{max} = 60 \text{ s}^{-1}$ $T_{max} = 2000 \text{ N}$ $Q_{max} = 100 \text{ Nm}$

The cavitation inception tests were carried out from $\lambda = 4.4$ to $\lambda = 8.9$, following the ITTC standards for cavitation tests [29]. Due to the high cross-sectional blockage ratio of 27%, a blockage correction had to be applied in the cavitation tunnel to match the operation points at free flow conditions. Cavitation inception was triggered by decreasing the static pressure, coming from a non-cavitating condition. Cavitation inception was identified visually.

The agreement between predicted and measured power and thrust coefficient characteristics is satisfactory, Fig. 7. The predicted inception of cavitation agrees well with the observed onset of cavitation related performance drop during the towing tank tests. The experimentally obtained $\sigma_{0.7,crit}(\lambda)$ values were somewhat smaller than the predicted characteristic, i.e. a conservative estimation. Hence, for the purpose of this work the semi-analytical performance prediction is regarded as validated. Further details of this and a second validation campaign are given in [19].

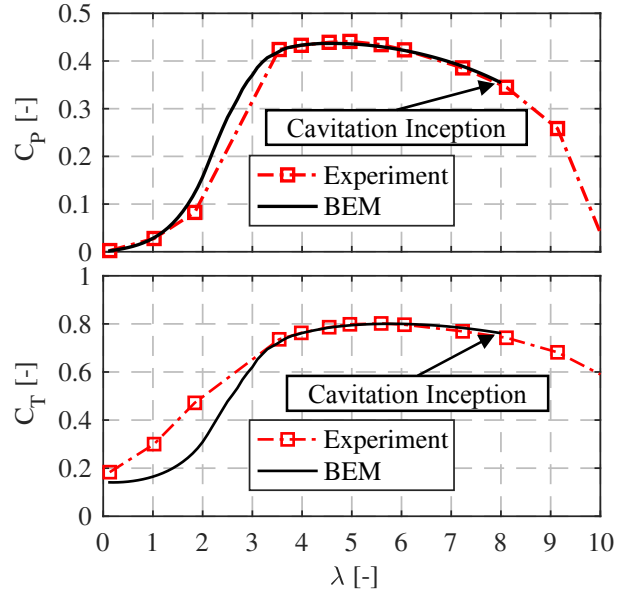


Fig. 7: 1:8 scaled model of the SCHOTTEL HYDRO Instream Turbine 250 (SIT250); upper: BEM-predicted power coefficient C_p vs. tip speed ratio λ and comparison with experimental data; lower: BEM-predicted thrust coefficient C_T vs. tip speed ratio λ and comparison with experimental data.

B. Multi-Objective Optimization: Parameters and Objective Functions

The parameters to be varied within the multi-objective optimization are the blade's spanwise chord length and twist angle distributions $l(r)$ and $\gamma(r)$, respectively, Fig. 8.

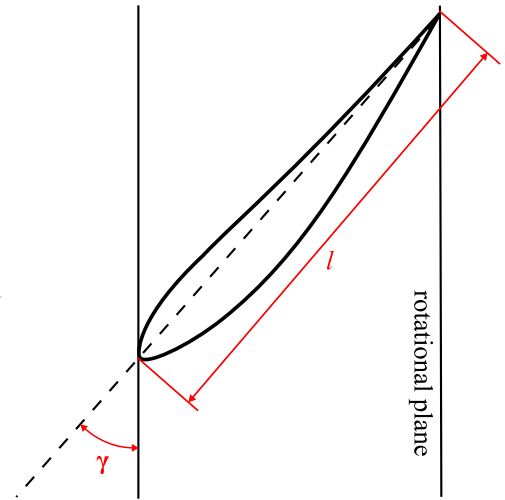


Fig. 8 Optimization parameter at a blade element (schematically)

They are parameterized through cubic Bézier curves to enable a high level of geometrical flexibility while keeping the number of parameters small. The radial positions of the resulting eight Bézier points (four per curve) are fixed, while

the l and γ values are varied during the optimization. For the presented work, the values at the hub were kept constant due to a given geometrical interface with the nacelle.

Beforehand, and hence not included in this multi-objective optimization scheme, the hydrofoil shapes have been created using another optimization workflow (similar as by GRASSO in [20]). For structural reasons the maximum thicknesses of the hydrofoil sections was fixed to 30% of the chord length at the hub and decreased to 13.7% at the tip. For the hub part ($r/r_{tip} < 0.5$), the hydrofoil shapes have been optimized to provide a maximum lift to drag ratio within the expected operating range. For blade elements closer to the rotor tip, the optimization also aimed at a reduction of the suction peaks to enlarge the non-cavitating operating range. Due to commercial interests, further details of the hydrofoils cannot be given.

Prior to an optimization a design inflow velocity c_0 is fixed. Each performance characteristic is parameterized at two tip speed ratios λ_1 and λ_2 . λ_1 is the design tip speed ratio for $c_0 < c_{0, rated}$, λ_2 an arbitrarily chosen shape control parameter. The first objective function becomes

$$obj_1 \equiv C_P(\lambda_1), \quad (5)$$

that has to be maximized to find the highest possible C_P at λ_1 . It should be mentioned, that λ_1 not necessarily equals λ_{opt} of the resulting turbine due to the repercussion of the other objectives. The second objective function λ_2 is

$$obj_2 \equiv C_T(\lambda_2), \quad (6)$$

that has to be minimized in order to reduce the thrust in overspeed operating points. Since cavitation should be avoided at any operating point, the third objective function, to be minimized as well, is

$$obj_3 \equiv 0.5(\sigma_{0.7, crit}(\lambda_1) + \sigma_{0.7, crit}(\lambda_2)). \quad (7)$$

Optimizing conflicting objectives results in a set of optimal solutions rather than one single optimal blade geometry. A solution set is called *Pareto-optimal*, if no objective of the set can be improved without a degradation of at least one other objective (see e.g. FONSECA and FLEMING [21]). Further information is needed, such as specific restrictions, to the suitable optimal solution from the *Pareto-set*.

C. Evolutionary Algorithm

The optimization is performed with an in-house evolutionary algorithm (EA). A detailed description of the code is given by BAMBERGER [22]. In many respects, the implementation follows the suggestions by FONSECA and FLEMING [21] as documented by THÉVENIN and JANIGA [23]. The algorithm applies three basic operators, *selection*, *crossover*, *survival* and *mutation*, to a population of blades geometries (*individuals*) to achieve an evolution of the turbine

performance over a number of iterations (*generations*). To enable multi-objective optimization, the selection operator by BAMBERGER has been extended by the sorting method of the *non-dominated sorting genetic algorithm NSGA-II* by DEB et al [13].

Starting with an initial population of the size n_P , the selection operator determines the individuals which are taken for the development of the following generation (*offspring*), based on their respective objective function values obj_n (with $n = 1, 2, 3$). The NSGA-II sorting uses the concepts of *dominance* and *diversity*.

Dominance: An individual x_i of a set S dominates the individual x_j of the same set if

- all objective function values $obj_{n,i}$ of x_i are at least equally good as compared to the objective function values $obj_{n,j}$ of x_j and
- at least one objective function value $obj_{n,i}$ is superior to the corresponding objective function value $obj_{n,j}$.

The number of individuals by which an individual x_i is dominated yields its non-domination rank R_i , where $R = 1$ relates the individuals which are not dominated by another individual (non-dominated).

Diversity: Subsequently, the individuals of each non-domination rank are sorted with respect to the spread, to favor solutions of less crowded regions of the objective space. Thus, individuals of same rank R are sorted such that an individual x_i with a larger distance to its neighbors in the objective space is graded higher than individual x_j of a more crowded region. Based on the resulting sorting, the best individuals (the number equals the population size n_P) are selected to generate the offspring.

To produce the individuals of the following generation, *crossover* is applied in a first step. The crossover operator randomly mixes the parameters (*genes*, here Bézier points) of two parent individuals to create the offspring. A random and moderate *mutation* is applied to all individuals produced by crossover to enlarge the investigated parameter space. The maximum mutation of a parameter is limited to a percentage (mutation magnitude Δm) of the parameter range of the respective generation. All non-dominated individuals are passed unchanged (*survival*) to the offspring since they represent the current optimum. If the number of non-dominated individuals exceeds 80% of the population size, the survival of the non-dominated is suspended for one offspring generation to enable a new gene pool and to avoid local optima. When the maximum number of generations is reached, the non-dominated geometries of all $n_P \cdot n_G$ investigated individuals are determined. While all elements of a true Pareto-set are non-dominated, the non-dominated members of a finite set are not necessarily Pareto-optimal [21]. Even though the true Pareto-set of the presented optimization task is unknown and the investigated parameter space is finite, the optimization result is called Pareto-set for simplicity. Table III summarizes the settings chosen for running the evolutionary algorithm.

TABLE II
OPTIMIZATION SETTINGS

Parameter	Value
Population Size n_P	1000
Number of Generations n_G	500
Mutation Probability p_m	100 %
Mutation Magnitude Δm	35 %

IV. RESULTS

A. Case study

As a case study the optimization of the blade for a turbine rotor with a diameter $d_{tip} = 6.3$ m, hub diameter $d_{hub} = 0.36$ m, inflow velocity $c_0 = 1.9$ m/s and a rated power $P_{rated} = 85$ kW is demonstrated. The design tip speed ratio was set to $\lambda_1 = 6$ and the off-design point to $\lambda_2 = 1.5 \cdot \lambda_1 = 9$.

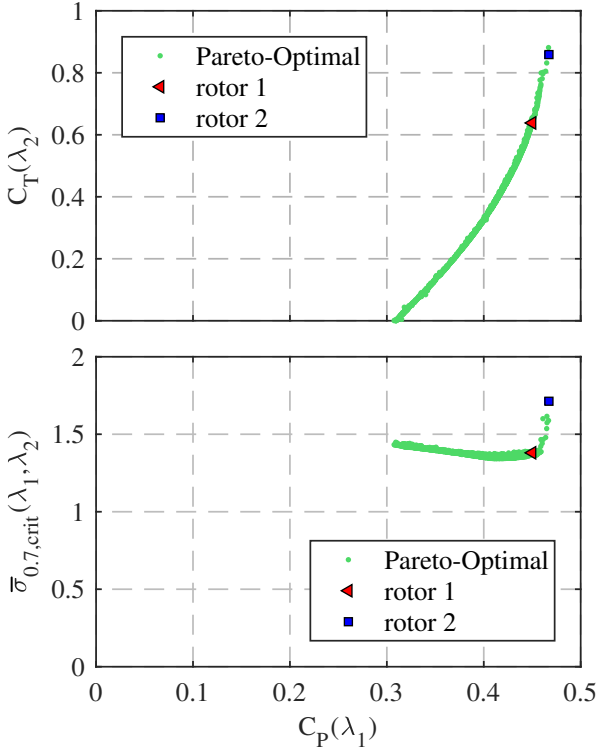


Fig. 9 Upper: projection of the objective space onto the C_P - C_T plane (black dots); lower: Projection of the objective space onto the C_P - $\sigma_{0.7,crit}$ plane (black dots). The positions of two exemplary blade geometries are depicted

Fig. 9 shows the objective space of the Pareto-set as result of the multi-objective optimization, projected to the C_P - C_T and C_P - $\sigma_{0.7,crit}$ plane, respectively. While the objective space for three objectives is in general a surface, the presented optimization result collapses to a thin band, implying that thrust reduction and cavitation avoidance can be achieved through similar designs. The 2D depiction of the objective space enables an evaluation of the trade-off between the restricting objectives (C_T and $\sigma_{0.7,crit}$) and the power

coefficient. The steep slopes close to the maximum of C_P imply that accepting a slightly lower power output offers a significant improvement of the further design targets.

Two blade geometries of the Pareto-set were chosen, rotor 1 and 2, for further analyses. While rotor 2 provides the highest C_P -value of all designs, i.e. it represents the maximum achievable power output, rotor 1 was selected to reveal the benefits when allowing a slightly less C_P .

For comparison a hypothetical benchmark rotor (rotor 3) was designed based on the traditional GLAUERT and SCHMITZ's theory (see e.g. GERHARD et al [24]). A design tip speed ratio $\lambda_D = 6$ was chosen. The angle of attack is set for the maximum lift to drag ratio at each blade element. The same hydrofoils and BE definition as for the optimization cases are used. Recall that GLAUERT/SCHMITZ exclusively aims at a maximum power extraction from each BE.

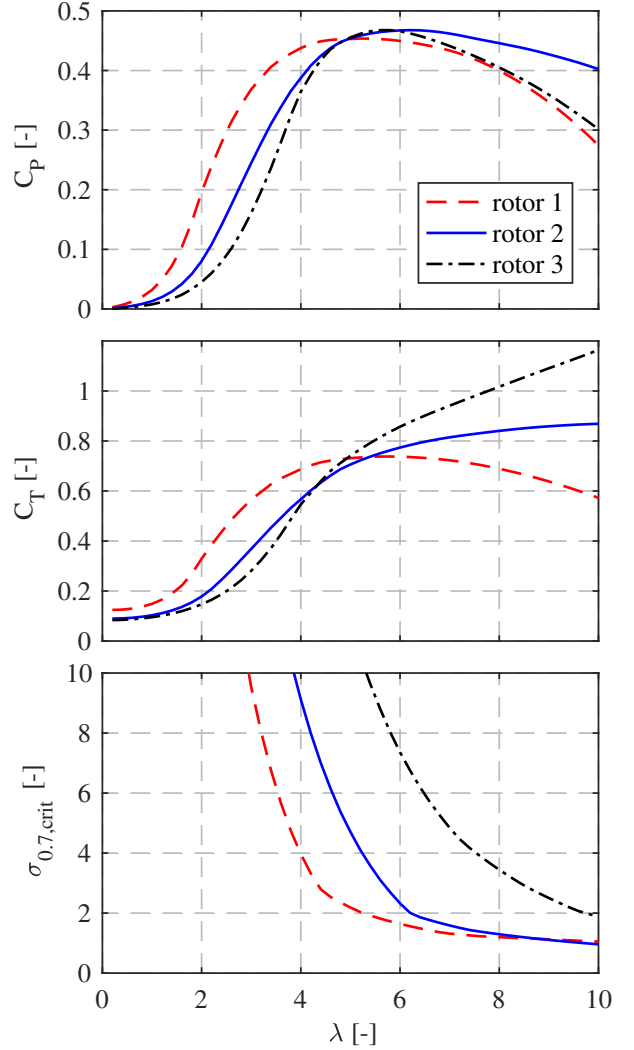


Fig. 10 Optimized turbine rotors (rotor 1 and 2) and benchmark rotor 3: predicted characteristics.

Fig. 10 shows a comparison of the predicted characteristics of two optimized versions and the benchmark turbine. While

providing the same C_p value at design tip speed ratio, the optimized rotor 2 has a significantly slower increasing thrust coefficient as compared to rotor 3. At $\lambda_2 = 1.5 \cdot \lambda_1 = 9$ the thrust of rotor 3 is 28% higher as compared to rotor 2 ($C_T(\lambda_2) = 1.1$ vs. 0.86). An even more substantial benefit is achieved for the critical cavitation number. Again comparing to rotor 2 which provides a similar power output, the critical cavitation number of rotor 3 is 216 % and 118 % larger at $\lambda_1 = 6$ and $\lambda_2 = 9$, respectively). Comparing rotor 1 and 2 shows that accepting a reduced power output of approximately 4% ($C_p(\lambda_1) = 0.45$ vs. 0.47) yields a thrust decrease of approximately 25% ($C_T(\lambda_2) = 0.64$ vs. 0.86).

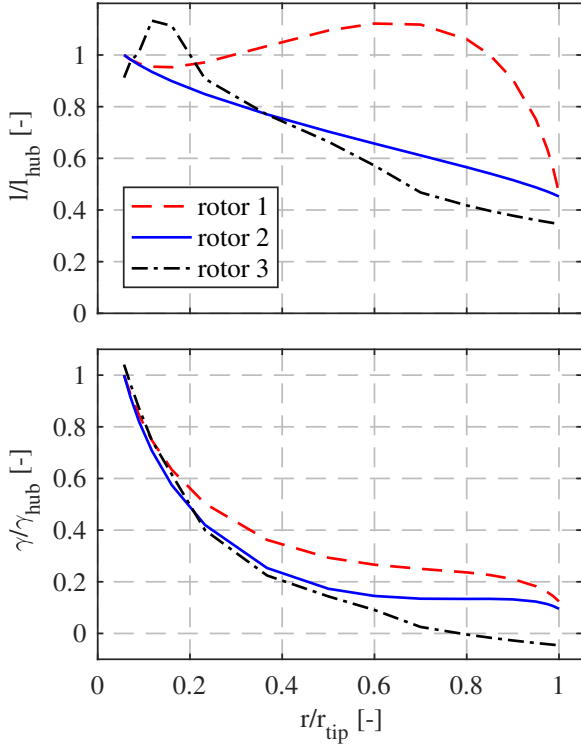


Fig. 11 Optimized turbine rotors (rotor 1 and 2) and benchmark rotor 3: blade geometry parameters along the span normalized with their value at the hub; upper: chord length, lower: twist angle

As a summary, the optimization yield a blade design (rotor 2) providing the same power coefficient at the design tip speed ratio as the traditional GLAUERT/SCHMITZ method but with lower thrust coefficient and cavitation numbers. A further improvement of the last two properties can be achieved if a slightly lower power coefficient is accepted as the comparison with the characteristics of rotors 1 and 2 reveals. Especially the decreasing thrust coefficient for high tip speed ratios is desirable for overspeed controlled turbines. The advantage regarding cavitation number of the rotor 1 over 2 is less distinctive for the relevant operating points ($\lambda_1 \leq \lambda$).

Fig. 11 depicts the associated blade geometries, found by the optimization and being eventually responsible for the turbine characteristics. To lower $\sigma_{0.7,crit}$ the optimizations results in an increase of twist angles which leads to smaller

angles of attack, hence to a reduced pressure peak on the blades suction side. Thus the chord length has been increased to compensate for the reduced pressure differential between suction and pressure side. With increasing chord length, the losses due to friction rise such that the compensation through a larger surface causes reduced C_p (rotor 1).

Fig. 12 shows the effect of the optimization on the steady points of operation over a varying inflow velocity. The higher C_T values of rotor 3 result in a larger thrust in the entire operating range in comparison to rotor 2 which provides the same power for the same inflow velocities. The decreasing $C_T(\lambda)$ slope of rotor 1 yields a slower increasing thrust at overspeed conditions, resulting in significant lower thrust as compared to rotor 2 and 3. In return, the power output of rotor 1 is lower for $\lambda = \lambda_1$ and P_{rated} is reached at a higher inflow velocity, as a result of the reduced $C_p(\lambda_1)$ value.

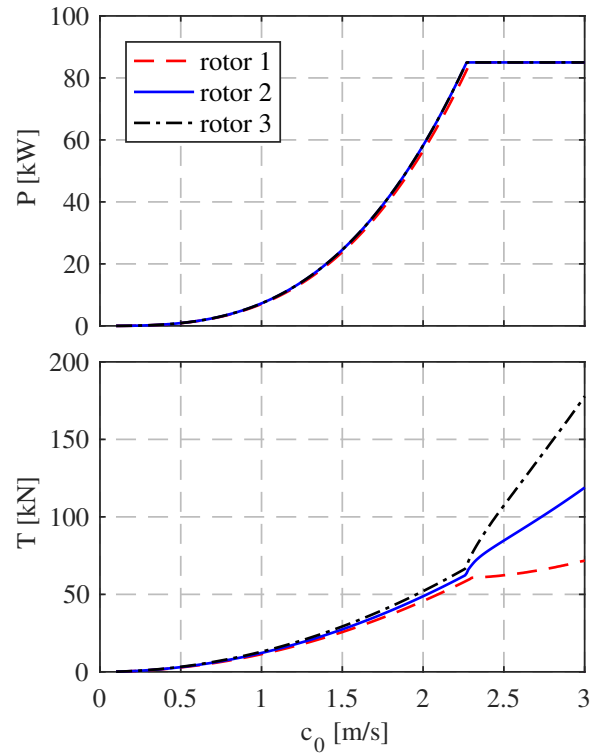


Fig. 12 Optimized turbine rotors (rotor 1 and 2) and benchmark rotor 3: points of steady operation for an overspeed controlled turbine, power output (upper) and thrust loads (lower) as function of the inflow velocity

To illustrate the impact of the critical cavitation number on the cavitation sensitivity of a fixed pitch turbine, the minimum immersion depth of the hub $h_{hub,min}$, representing the threshold to cavitating operating points, are shown as function of the inflow velocity, Fig. 13. In order to avoid effects through surface interaction, a minimum hub immersion depth of d_{tip} is considered. The comparison of the three rotors display the tendencies expected from their respective critical cavitation numbers. Rotor 3 has to be immersed substantially deeper to operate without cavitating for the same inflow velocities compared to the optimized rotor designs. In the case of rotor 3, the change of the slope at overspeed conditions illustrates the

positive effect of a decreasing $\sigma_{0.7,crit}/\lambda$ curve for $\lambda > \lambda_1$. Again, accepting less power output results in an improvement of a conflicting design target: rotor 1 can operate at shallower immersion depths as compared to rotor 2.

As a intermediate conclusion the optimization improves the turbine performance particularly in overspeed conditions, i.e. the method is addressing the design targets determined essentially by the variable speed control strategy. Nevertheless there is still a positive effect at the design point ($\lambda = \lambda_1$).

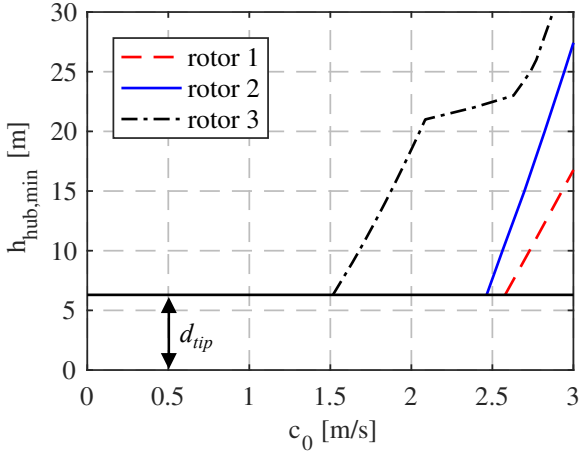


Fig. 13 Optimized turbine rotors (rotor 1 and 2) and benchmark rotor 3: minimum immersion depths of the hub for cavitation free operating conditions as function of the inflow velocity.

B. Effect of the Chosen Design Tip Speed Ratio

For the previously discussed optimization the tip speed ratios λ_1 and λ_2 were arbitrarily chosen. The choice of the values of those parameters, however, affects the optimization results. To evaluate this effect, λ_1 was varied from 4 to 9, with the off design tip speed ratio accordingly: $\lambda_2 = k \cdot \lambda_1$, where factor k was varied in the range of $1 \leq k \leq 2.5$.

Fig. 14 depicts the upper limit of the power coefficient for the different design tip speed ratios. From the maximum of 0.47 at 6 and 7, the $C_{P,max}(\lambda_1)$ values decrease towards smaller and higher tip speed ratios. The decline towards lower tip speed ratios is caused by more energy in the rotating wake, which cannot be recovered. The decrease of $C_{P,max}(\lambda_1)$ for $\lambda_1 > 7$ most probably results from rising losses through friction due to the higher relative velocities at the blades. Hence, a reduction of the blade number could be beneficial for high design tip speed ratios, since the overall wetted surface is decreased.

As a summary, the arbitrary selection of $\lambda_1 = 6$ turned out to be a good choice, since it obviously allows the maximum of the achievable power output.

V. SUMMARY AND CONCLUSIONS

The objectives of this contribution was an enhanced design method of 3D blade geometries for fixed pitch horizontal axis tidal turbines with variable speed control, simultaneously targeting at

- maximum power output,
- minimum thrust load and
- an extended cavitation free range of operation.

To optimize the blade's spanwise twist and chord distribution, an enhanced BEM code, allowing the prediction of the performance characteristics including cavitation inception, was coupled to an evolutionary algorithm, capable of global multi-objective optimization. The major benefit of the multi-objective optimization is, that - upon a single creation of a Pareto-optimal geometry set - a designer can simply select the geometry which represents the best suitable trade-off between the conflicting design targets. Thus, no further optimization runs are required when the specifications change during the design process.

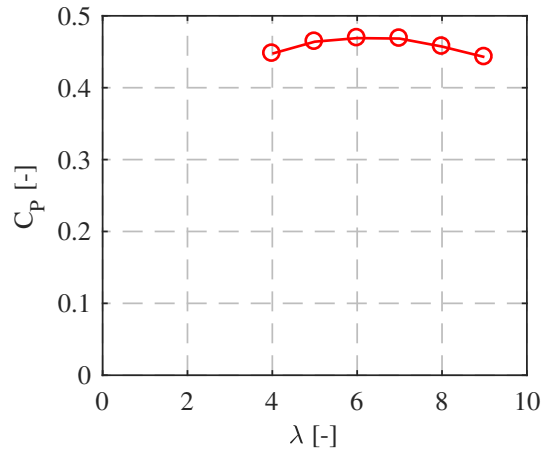


Fig. 14 Maximum achieved power coefficient of the multi-objective optimization as a function of the design tip speed ratio chosen.

A design case study was performed resulting in a set of novel blade geometries, providing optimum trade-offs between power coefficient, thrust coefficient and critical cavitation number. The comparison to an analytically designed rotor using the traditional GLAUTERT/SCHMITZ method showed that the presented optimization method yields rotor geometries with significantly lower thrust loads and cavitation sensitivity as compared to the analytical blade design.

The comparison with an analytically designed rotor method showed that the presented optimization method yields a rotor geometry with significantly lower thrust and improved cavitation sensitivity.

Results of any optimization depend strongly on the choice of the design point. Design tip speed ratios of 6 and 7 provided the highest power output.

As already pointed out BEM predictions may be less accurate than high fidelity CFD-methods. The successful validation of the prediction model, however, was encouraging for this work: embedding the performance prediction model in

a multi-objective optimization scheme. There is a general trade-off: simple but numerically stable models vs. a high level of detail. The low demand of computational power and the stability of its solutions argue for the semi-analytical BEM performance prediction as a key component in the novel scheme. Yet, a validation of the presented design method through experiments is unavoidable and will be carried out in the near future.

ACKNOWLEDGMENT

This work has been funded by the Federal Ministry for Economic Affairs and Energy of Germany (BMWi) in the project TIDAL POWER (FKZ 0325817B). The results of the model scale test were provided by SCHOTTEL HYDRO GmbH.

REFERENCES

- [1] (2017) SCHOTTEL Hydro website. [Online]. Available: <http://www.schottel.de/schottel-hydro/sit-instream-turbine/>
- [2] Glauert, H.: *Airplane propellers*. ser: Aerodynamic Theory, Berlin, Germany, Springer, 1935, 169-360
- [3] Schmitz, G., "Theorie und Entwurf von Windrädern optimaler Leistung". *Wiss. Zeitung der Universität Rostock*, 5. Jahrgang 1955/56
- [4] Batten, W., Bahaj, A. S., Molland, A. F., Chaplin, J. R.: "The prediction of the hydrodynamic performance of marine current turbines". *Renewable Energy* vol. 33, Iss. 5, pp. 1085–1096, May 2008
- [5] Masters, I., Chapman, J. C., Wilis, M. R., Orme, J.: "A Robust Blade Element Momentum Theory Model for Tidal Stream Turbines Including Tip and Hub Loss Corrections". *Journal of Marine Engineering and Thechnology*, vol. 10, Iss.1, pp. 25–35, Jan. 2011
- [6] da Silva, P., Shinomiya, L., et al, "Design of Hydrokinetic Turbine Blades Considering Cavitation", *Energy Procedia*, vol. 75, pp. 277–282, Aug. 2015.
- [7] Goundar, J. N. and Ahmed, M. R., "Design and Optimization of a Horizontal Axis Marine Current Turbine," *Applied Energy*, no. 111, pp. 161–174, 2013
- [8] Wu, B., Zhang, X., et al, "Design of high-efficient and universally applicable blades of tidal stream turbine," *Energy*, vol. 60, pp. 187–194, 2013.
- [9] Arnold, M.; Biskup, F. and Cheng, P. W., "Load reduction potential of variable speed control approaches for fixed pitch tidal current turbines," *International Journal of Marine Energy*, vol. 15, pp. 175-190, Sept. 2016.
- [10] D. Sale, J. Jonkman, W. Musial, "Hydrodynamic Optimization Method and Design Code for Stall-Regulated Hydrokinetic Turbine Rotors". in *Proc. ASME 28th International Conference on Ocean, Offshore, and Arctic Engineering*, Honolulu, Hawaii. 31 May to 5 June 2009
- [11] Ruopp, A. Ruprecht, A., "Automatic Blade Optimisation of Tidal Current Turbines Using OpenFoam", in *Proc. 9th European Wave and Tidal Energy Conference (EWTEC)*, Southampton, UK, 2013
- [12] Huang, B. and Kanemoto, T., "Multi-objective numerical optimization of the front blade pitch angle distribution in a counter-rotating type horizontal-axis tidal turbine," (en), *Renewable Energy*, vol. 81, pp. 837–844, Apr. 2015.
- [13] Deb, K.; Pratap, A.; Agarwal, S. and Meyarivan, T., "A fast and elitist multiobjective genetic algorithm: NSGA-II," *IEEE Trans. Evol. Computat*, vol. 6, no. 2, pp. 182–197, Apr. 2002
- [14] Buhl, M. L., "New Empirical Relationship between Thrust Coefficient and Induction Factor for the Turbulent Windmill State". National Renewable Energy Laboratory, Tech. Rep. NREL/TP-500-36834. 2005
- [15] Shen, W. Z., Mikkelsen, R., Sørensen, J. N., Bak, C.: Tip loss corrections for wind turbine computations. *Wind Energy*, vol. 8 Iss. 4, pp. 457–475, 2005
- [16] Drela, M. (2013) XFOIL - Subsonic Airfoil Development System. [Online] Available: <http://web.mit.edu/drela/Public/web/xfoil/>.
- [17] Drela, M.: XFOIL: An Analysis and Design System for Low Reynolds Number Airfoils. In: *Low Reynolds Number Aerodynamics*. Proceedings of the Conference Notre Dame, Indiana, USA, 5-7 June 1989. Lecture Notes in Engineering, Bd. 54. Berlin, Heidelberg: Springer 1989, 1–12
- [18] Viterna, L. A., Corrigan, R. D.: "Fixed pitch rotor performance of large horizontal axis wind turbines". in *Proc. DOE/NASA workshop on large HAWTs*. 1981
- [19] Kaufmann, N., Carolus, T.H., Starzmann, R., "An Enhanced and Validated Performance and Cavitation Prediction Model for Horizontal Axis Tidal Turbines". Institute for Fluid- and Thermodynamics, University of Siegen, Internal Report No. B84_002, 2016
- [20] Grasso, F., "Design and Optimization of Tidal Turbine Airfoil," *Journal of Aircraft*, vol. 49, no. 2, pp. 636–643, Mar.-Apr. 2012.
- [21] Fonseca, C. M., Fleming, P. J., 1993, "Genetic Algorithms for Multiobjective Optimization: Formulation, Discussion and Generalization", in *Proc. Genetic Algorithms: Proceedings of the Fifth International Conference*, Jul. 1993.
- [22] Bamberger, K., "Aerodynamic Optimization of Low-Pressure Axial Fans", PhD Thesis, Institute for Fluid- and Thermodynamics, University of Siegen, Nov. 2015
- [23] Thévenin, D., Janiga, G., *Optimization and Computational Fluid Dynamics* Heidelberg, Germany. Springer Verlag GmbH, 2008
- [24] Gerhard, T., Carolus, T., "Sturm, M.: Small horizontal axis wind turbine: Analytical blade design and comparison with RANS-prediction and first experimental data". in *Proc. of the ASME Turbo Expo: Turbine Technical Conference and Exposition*, 2013